CAN QCD-ENERGY-SCALE-TURBULENCE SOURCED GRAVITATIONAL WAVES BE DETECTED THROUGH PTAs?

TINA KAHNIASHVILI

CARNEGIE MELLON UNIVERSITY & ILIA STATE UNIVERSITY

DPF-PHENO 2024

15 MAY, 2024

COLLABORATION

- AXEL BRANDENBURG, LEONARDO CAMPANELLI, RUTH DURRER, GIGA GOGOBERIDZE, ARTHUR KOSOWSKY, ANDRII NERONOV, BHARAT RATRA, ALEXANDER TEVZADZE, TANMAY VACHASPATI
- EMMA CLARKE, CLAIRE HUANG, ANDREW MACK, SAYAN MANDAL, SALOME MTCHEDLIDZE, ALBERTO ROPER POL, JONATHAN STEPP, GUITONG SUN, WINSTON YIN
- ANDREW LONG, PHILIP MOCZ, JENNIFER SCHOBER, MARK VOGELBERGER…

Connection with High Energy Particle Physics – the best laboratory to test the energy scales EVEN near the Planck scale

- The very early universe (inflation)
- Topological defects/strings
- Cosmological phase transitions
  - Bubble nucleation/collisions
  - Sound waves
  - Hydro turbulence
  - MHD turbulence

Garcia Bellido et al. 2020

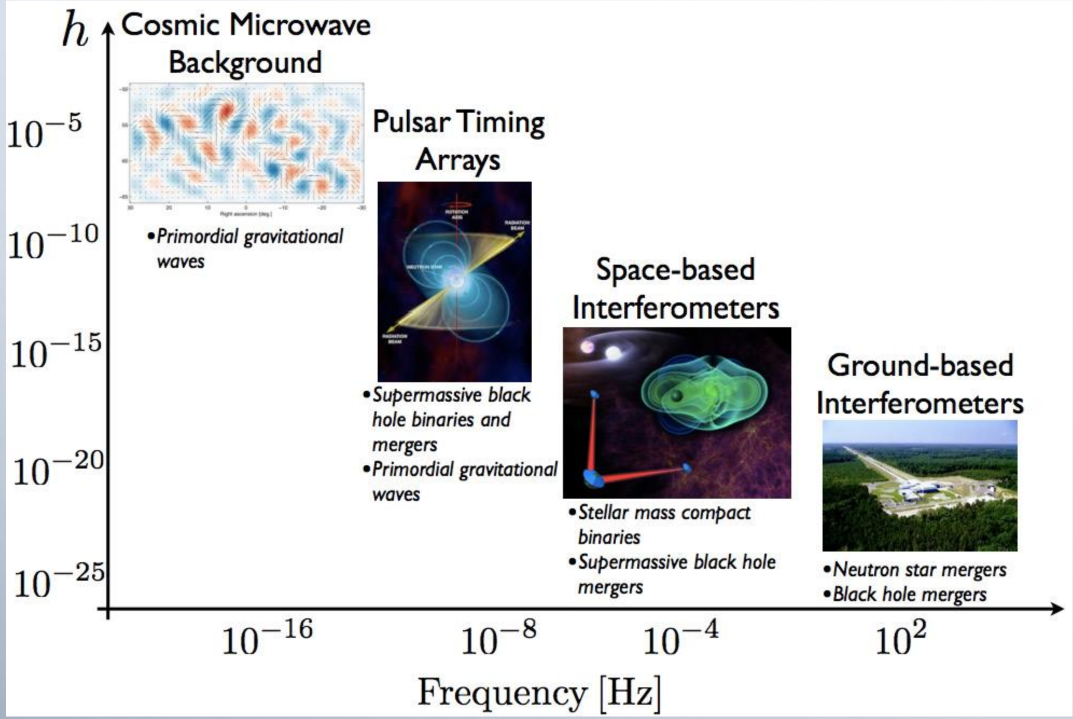

Credit: NANOGrav

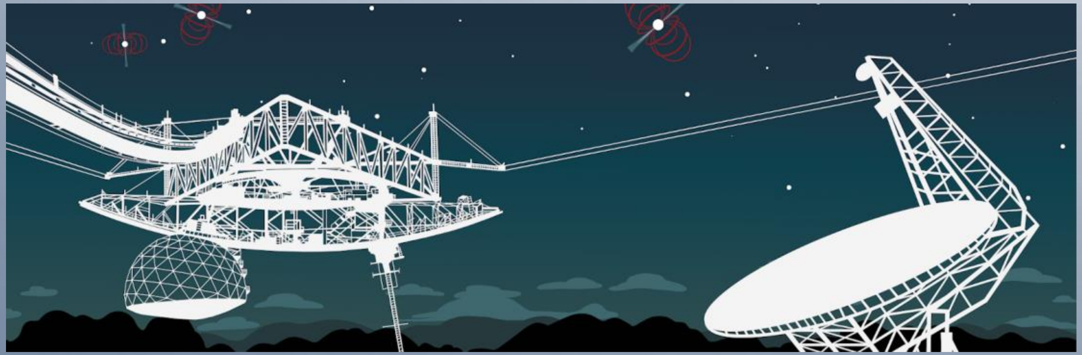

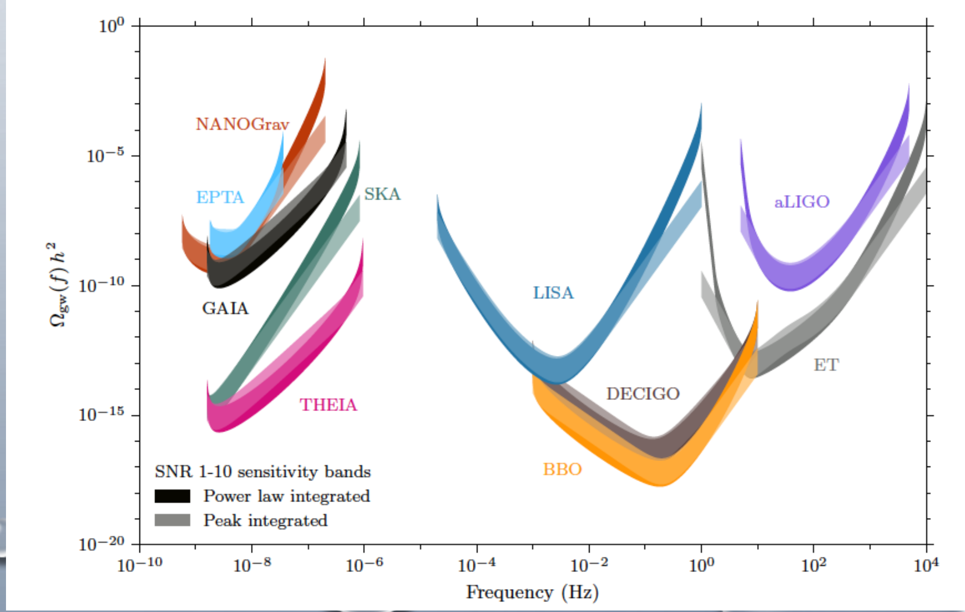

EARLY UNIVERSE – GRAVITATIONAL WAVES

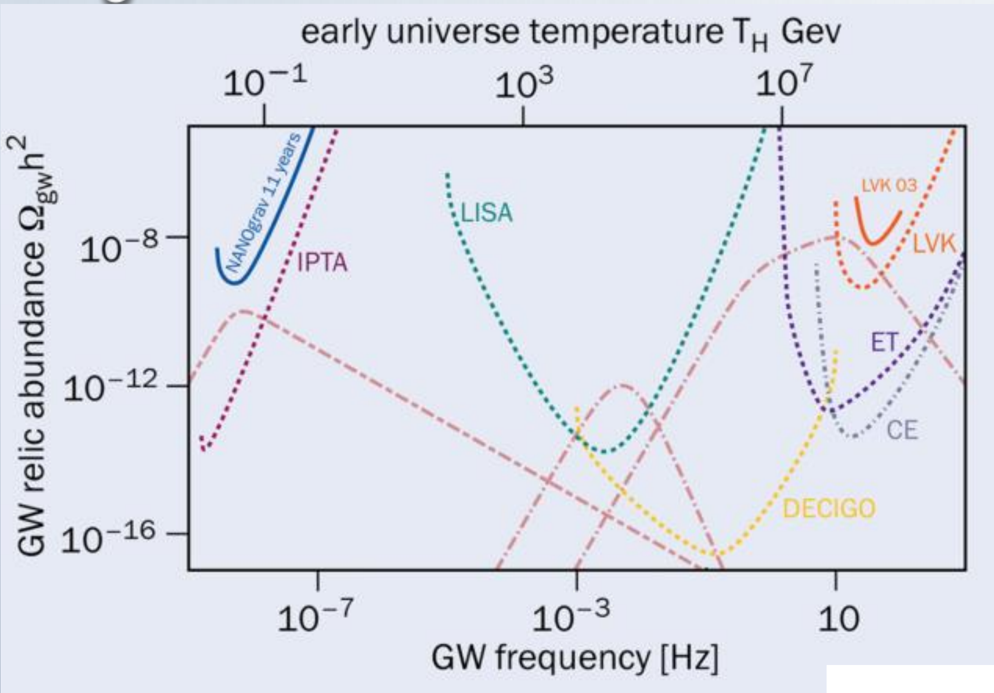

$$\Omega_{\rm GW}(t,f) = \frac{1}{\mathcal{E}_{\rm crit}(t)}\frac{{\rm d}\mathcal{E}_{\rm GW}}{{\rm d}\ln f}$$

Credit: CERN Courier, 2021

Sensitivity of current (solid) and future (dashed) gravitational-wave (GW) observatories to stochastic GW backgrounds (expressed in terms of the energy density fraction in the universe today). On the upper x-axis, the temperature in the early universe is given, which is obtained when the peak frequency of a GW signal is equal to the inverse of the expansion rate when GWs are emitted. Some example possible GW spectra from the early universe are also shown (pink, dashed). F. Rompineve/ arXiv:2101.12130/arXiv:2002.0461

The Astrophysical Journal Letters, 951:L8 (24pp), 2023 July 1 — Agazie et al.

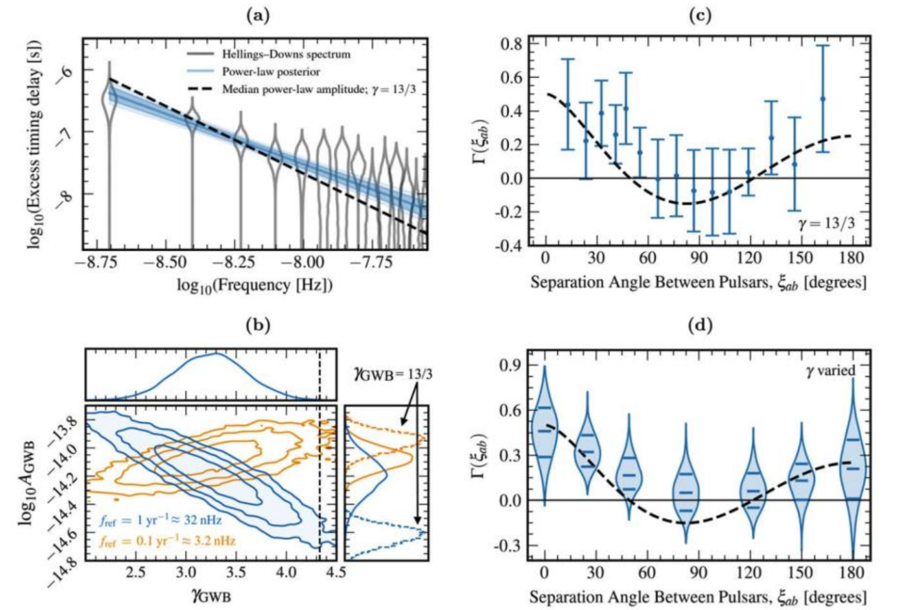

Figure 1. Summary of the main Bayesian and optimal-statistic analyses presented in this paper, which establish multiple lines of evidence for the presence of Hellings–Downs correlations in the 15 yr NANOGrav data set. Throughout we refer to the 68.3%, 95.4%, and 99.7% regions of distributions as $1\sigma/2\sigma/3\sigma$ regions, even in two dimensions. (a) Bayesian "free-spectrum" analysis, showing posteriors (gray violins) of independent variance parameters for a Hellings–Downs-correlated stochastic process at frequencies i/T, with T the total data set time span. The blue represents the posterior median and $1\sigma/2\sigma$ posterior bands for a power-law model; the dashed black line corresponds to a $\gamma = 13/3$ (SMBHB-like) power law, plotted with the median posterior amplitude. See Section 3 for more details. (b) Posterior probability distribution of GWB amplitude and spectral exponent in an HD power-law model, showing $1\sigma/2\sigma/3\sigma$ credible regions. The value $\gamma_{\rm GWB} = 13/3$ (dashed black line) is included in the 99% credible region. The amplitude is referenced to $f_{\rm ref} = 1\ {\rm yr}^{-1}$ (blue) and $0.1\ {\rm yr}^{-1}$ (orange). The dashed blue and orange curves in the $\log_{10}A_{\rm GWB}$ subpanel show its marginal posterior density for a $\gamma = 13/3$ model, with $f_{\rm ref} = 1\ {\rm yr}^{-1}$ and $f_{\rm ref} = 0.1\ {\rm yr}^{-1}$, respectively. See Section 3 for more details. (c) Angular-separation-binned interpulsar correlations, measured from 2211 distinct pairings in our 67-pulsar array using the frequentist optimal statistic, assuming maximum-a-posteriori pulsar noise parameters and $\gamma = 13/3$ common-process amplitude from a Bayesian inference analysis. The bin widths are chosen so that each includes approximately the same number of pulsar pairs, and central bin locations avoid zeros of the Hellings–Downs curve. This binned reconstruction accounts for correlations between pulsar pairs (Romano et al. 2021; Allen & Romano 2022). The dashed black line shows the Hellings–Downs correlation pattern, and the binned points are normalized by the amplitude of the $\gamma = 13/3$ common process to be on the same scale. Note that we do not employ binning of interpulsar correlations in our detection statistics; this panel serves as a visual consistency check only. See Section 4 for more frequentist results. (d) Bayesian reconstruction of normalized interpulsar correlations, modeled as a cubic spline within a variable-exponent power-law model. The violins plot the marginal posterior densities (plus median and 68% credible values) of the correlations at the knots. The knot positions are fixed and are chosen on the basis of features of the Hellings–Downs curve (also shown as a dashed black line for reference): they include the maximum and minimum angular separations, the two zero-crossings of the Hellings–Downs curve, and the position of minimum correlation. See Section 3 for more details.

Credit: NANOGrav 2023

$$\Omega_{\rm GW}(f) = \frac{2\pi^2}{3H_0^2}f^2h_c^2(f) = \Omega_{\rm GW}^{\rm yr}\left(\frac{f}{f_{\rm yr}}\right)^{5-\gamma_{\rm CP}}$$

NANOGRAV SIGNAL – POSSIBLE SOURCES

Astrophysical:

- ✓ Super massive black hole binary (SMBHB) (Phinney 2001): γ=13/3

Cosmological:

- ✓ Bubbles collisions (Kosowsky et. Al. 1993)
- ✓ Inflation (Vagnozzi 2020)
- ✓ Cosmic strings (Blanco-Pillado et al. 2020)
- ✓ Seed magnetic fields (Neronov et. al. 2020)
- ✓ Hydrodynamic and MHD Turbulence (Brandenburg et al. 2021)

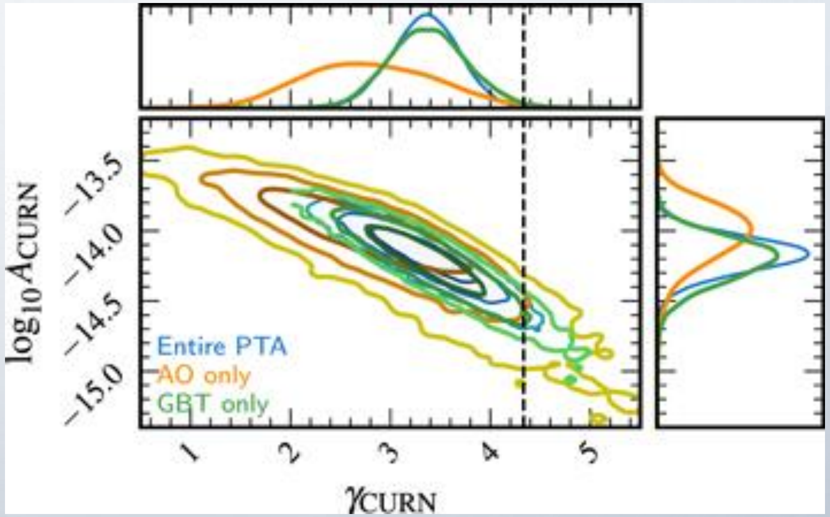

The NANOGrav 15 yr Data Set: Evidence for a Gravitational-wave Background

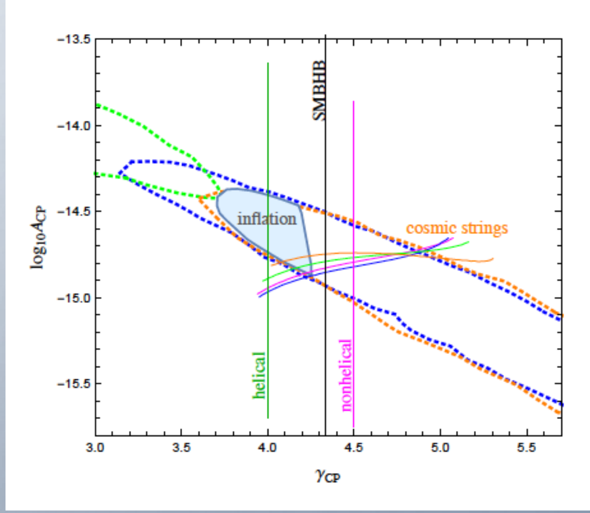

Clarke, et al. 2021

QCD energy scale

$$\frac{a_0}{a_\star} = 10^{12}\left(\frac{g_{S,\star}}{15}\right)^{\frac{1}{3}}\left(\frac{T_\star}{150\ \mathrm{MeV}}\right)$$

$$f_H \simeq (1.8 \times 10^{-8}\mathrm{Hz})10^{12}\left(\frac{g_\star}{15}\right)^{\frac{1}{3}}\left(\frac{T_\star}{150\ \mathrm{MeV}}\right)$$

$$H_\star^2 = \frac{8\pi G}{2}\mathcal{E}_{\mathrm{rad},\star} \qquad \mathcal{E}_{\mathrm{rad},\star} = \frac{\pi^2 g_\star}{30}T_\star^4 \qquad (c = k_B = \hbar = 1)$$

QCD PHASE TRANSITIONS – GRAVITATIONAL WAVES

Pulsar Timing Arrays (PTAs) are sensible to gravitational waves generated or present at QCD energy scales

Sazhin, 1978, Detweiler 1979

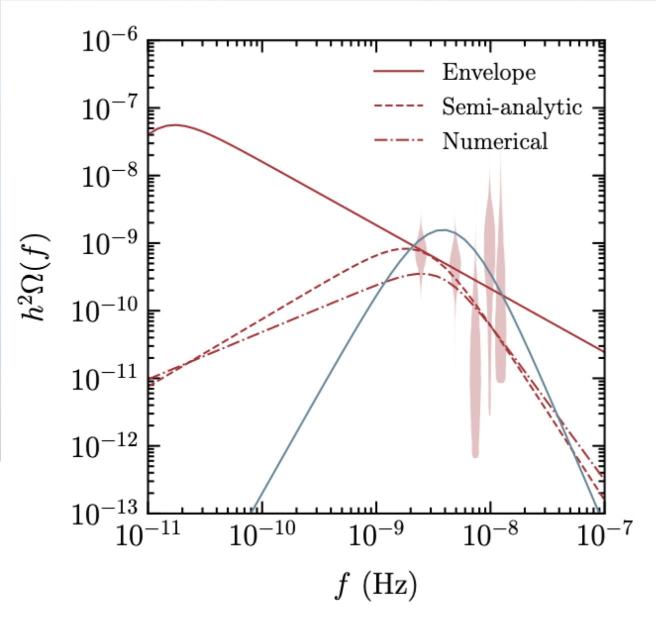

NANOGrav 12.5yr data

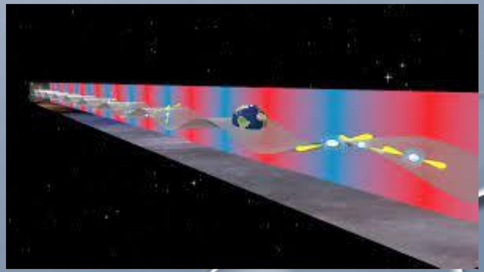

PHYSICAL REVIEW D VOLUME 49, NUMBER 6 15 MARCH 1994

Gravitational radiation from first-order phase transitions

Marc Kamionkowski*
School of Natural Sciences, Institute for Advanced Study, Princeton, New Jersey 08540

Arthur Kosowsky† and Michael S. Turner‡
NASA/Fermilab Astrophysics Center, Fermi National Accelerator Laboratory, Batavia, Illinois 60510-0500
and Departments of Physics and of Astronomy and Astrophysics,
Enrico Fermi Institute, The University of Chicago, Chicago, Illinois 60637-1433
(Received 26 October 1993)

We consider the stochastic background of gravity waves produced by first-order cosmological phase transitions from two types of sources: colliding bubbles and hydrodynamic turbulence. First we discuss the fluid mechanics of relativistic spherical combustion. We then numerically collide many bubbles expanding at a velocity v and calculate the resulting spectrum of gravitational radiation in the linearized gravity approximation. Our results are expressed as simple functions of the mean bubble separation, the bubble expansion velocity, the latent heat, and the efficiency of converting latent heat to kinetic energy of the bubble walls. A first-order phase transition is also likely to excite a Kolmogoroff spectrum of turbulence. We estimate the gravity waves produced by such a spectrum of turbulence and find that the characteristic amplitude of the gravity waves produced is comparable to that from bubble collisions. Finally, we apply these results to the electroweak transition. Using the one-loop effective potential for the minimal electroweak model, the characteristic amplitude of the gravity waves produced is $h \simeq 1.5 \times 10^{-27}$ at a characteristic frequency of 4.1×10^{-3} Hz corresponding to $\Omega \sim 10^{-22}$ in gravity waves, far too small for detection. Gravity waves from more strongly first-order phase transitions, including the electroweak transition in nonminimal models, have better prospects for detection, though probably not by LIGO.

Pioneering works:

- *Winicour 1973*
- *Hogan 1982, 1986*
- *Turner & Wilczek 1990*
- *Kosowsky, Turner, Watkins. 1992*

NANOGRAV & PHASE TRANSITIONS

PHYSICAL REVIEW LETTERS **127,** 251302 (2021)

Editors' Suggestion | Featured in Physics

Searching for Gravitational Waves from Cosmological Phase Transitions with the NANOGrav 12.5-Year Dataset

Zaven Arzoumanian,[1] Paul T. Baker,[2] Harsha Blumer,[3,4] Bence Bécsy,[5] Adam Brazier,[6,7] Paul R. Brook,[3,4] Sarah Burke-Spolaor,[3,4,8] Maria Charisi,[9] Shami Chatterjee,[6] Siyuan Chen,[10,11,12] James M. Cordes,[6] Neil J. Cornish,[5] Fronefield Crawford,[13] H. Thankful Cromartie,[6] Megan E. DeCesar,[14,15*] Paul B. Demorest,[16] Timothy Dolch,[17,18] Justin A. Ellis,[19] Elizabeth C. Ferrara,[20,21,22] William Fiore,[3,4] Emmanuel Fonseca,[23] Nathan Garver-Daniels,[3,4] Peter A. Gentile,[3,4] Deborah C. Good,[24] Jeffrey S. Hazboun,[25] A. Miguel Holgado,[26,27] Kristina Islo,[28] Ross J. Jennings,[6] Megan L. Jones,[28] Andrew R. Kaiser,[3,4] David L. Kaplan,[28] Luke Zoltan Kelley,[29] Joey Shapiro Key,[25] Nima Laal,[30] Michael T. Lam,[31,32] T. Joseph W. Lazio,[33] Vincent S. H. Lee,[34] Duncan R. Lorimer,[3,4] Jing Luo,[35] Ryan S. Lynch,[36] Dustin R. Madison,[3,4] Maura A. McLaughlin,[3,4] Chiara M. F. Mingarelli,[37,38] Andrea Mitridate,[34] Cherry Ng,[39] David J. Nice,[14] Timothy T. Pennucci,[40,41] Nihan S. Pol,[3,4,9] Scott M. Ransom,[40] Paul S. Ray,[42] Brent J. Shapiro-Albert,[3,4] Xavier Siemens,[30,28] Joseph Simon,[33,43] Renée Spiewak,[44] Ingrid H. Stairs,[24] Daniel R. Stinebring,[45] Kevin Stovall,[16] Jerry P. Sun,[30] Joseph K. Swiggum,[14] Stephen R. Taylor,[9] Jacob E. Turner,[3,4] Michele Vallisneri,[33] Sarah J. Vigeland,[28] Caitlin A. Witt,[3,4] and Kathryn M. Zurek[34]

(NANOGrav Collaboration)

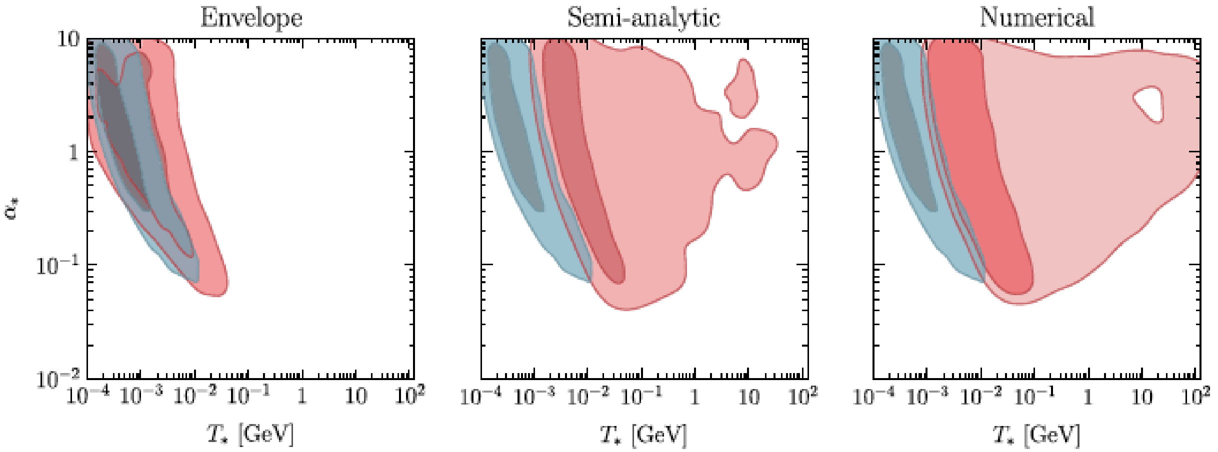

FIG. 1. In red (blue) the 1-σ (68% posterior credible level), and 2-σ (95% posterior credible level) contours for the two-dimensional posterior distributions in the (T_*, α_*) plane obtained in the BO (SWO). The BO analysis has been performed with the spectral shape computed by using the envelope approximation (left panel), semianalytic results (central panel), and numerical results (right panel). Specifically, we use $(a, b, c) = (1, 2.61, 1.5)$ for the semianalytic results, and $(a, b, c) = (0.7, 2.3, 1)$ for the numerical results.

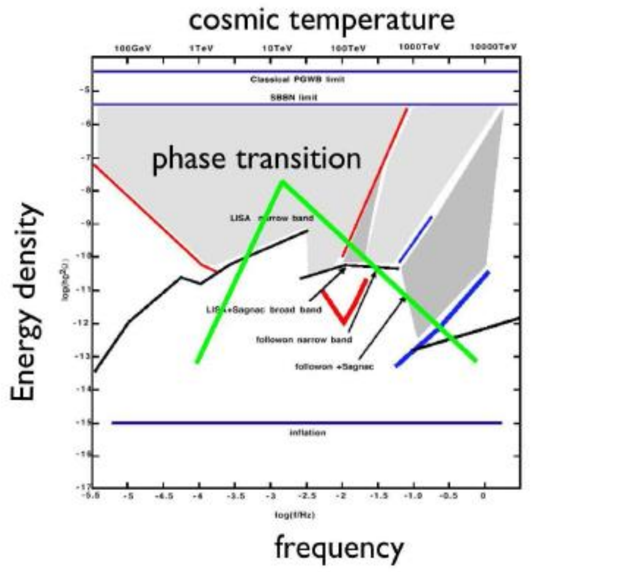

T_* [GeV]	Phase transition temperature
α_*	Phase transition strength
H_*/β	Bubble nucleation rate
v_w	Bubble wall velocity

TABLE I. Parameters for the gravitational wave spectrum of Eq. (4). The values of the parameters (a, b, c) in the spectral shape of the bubble contribution are reported in Table II.

	Bubbles [58]	Sound waves [59]
$\Delta(v_w)$	$[0.48 v_w^3/(1+5.3 v_w^2+5 v_w^4)]$	$0.513 v_w$
κ	κ_ϕ	κ_{SW}
p	2	2
q	2	1
$S(x)$	$\{(a+b)^c/[b x^{-a/c} + a x^{b/c}]^c\}$	$x^3[7/(4+3x^2)]^{7/2}$
f_*/β	$[0.35/(1+0.07 v_w + 0.69 v_w^4)]$	$(0.536/v_w)$

C. Hogan, 2006

GRAVITATIONAL WAVES – ANISOTROPIC STRESS

Mon. Not. R. astr. Soc. (1987) **229**, 357–370

$$\boldsymbol{\nabla}^2 h_{ij}(\boldsymbol{x},t) - \frac{\partial^2}{\partial t^2} h_{ij}(\boldsymbol{x},t) = -16\pi G\, S_{ij}(\boldsymbol{x},t)$$

Generation of gravitational waves by the anisotropic phases in the early Universe

D. V. Deryagin, D. Yu. Grigoriev and
V. A. Rubakov *Institute for Nuclear Research, USSR Academy of Sciences, Moscow 117312, USSR*
M. V. Sazhin *P. K. Sternberg Astronomical Institute, Universitetskii pr. 13, Moscow 119899, USSR*

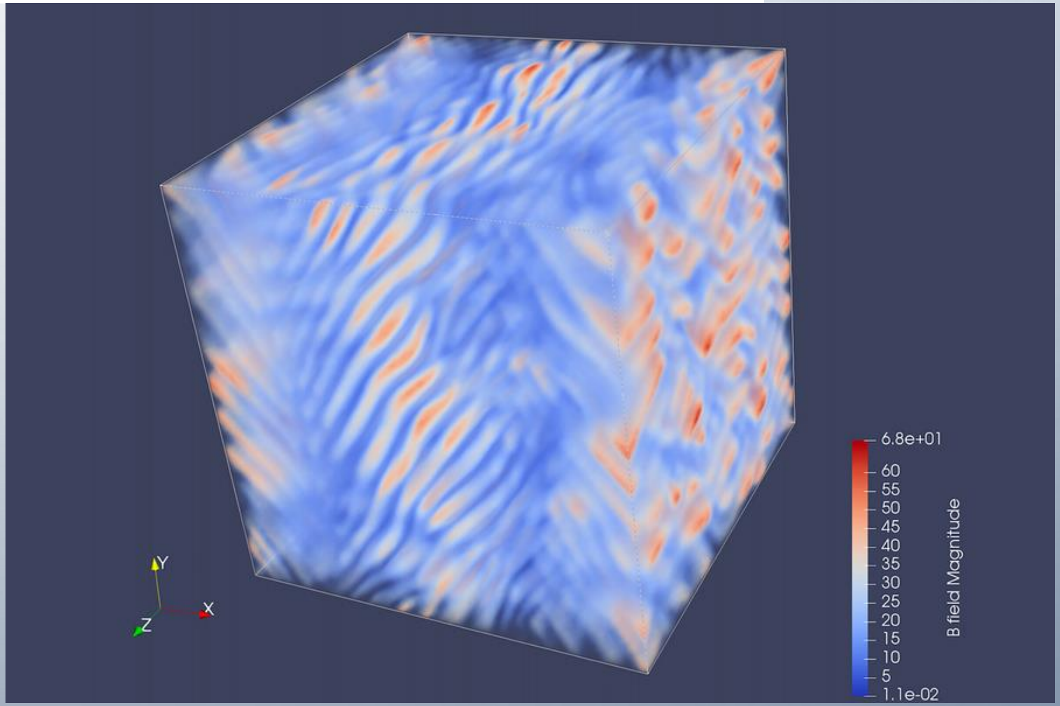

Greenwald, 2022

Magnetic fields;
Turbulence (hydro & MHD)

WHY PRIMORDIAL MAGNETIC FIELDS?

- cosmic *seed* magnetic fields
  - astrophysical seeds
  - cosmological seeds
- observations
  - Fermi data – blazars spectra

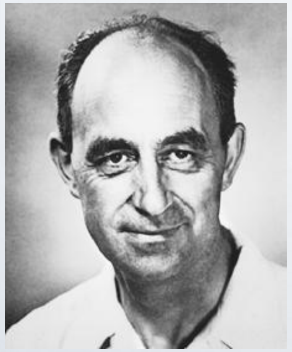

E. Fermi *“On the origin of the cosmic radiation”*, PRD, 75, 1169 (1949)

F. Hoyle in Proc. *“La structure et l’evolution de ’Universe”* (1958)

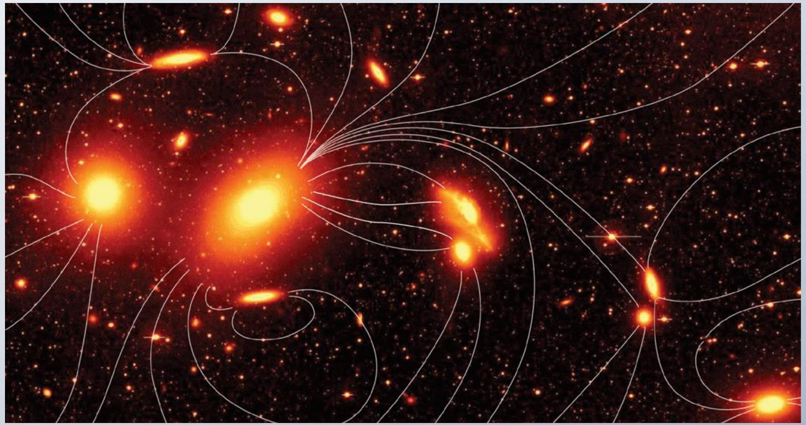

Durrer 2008

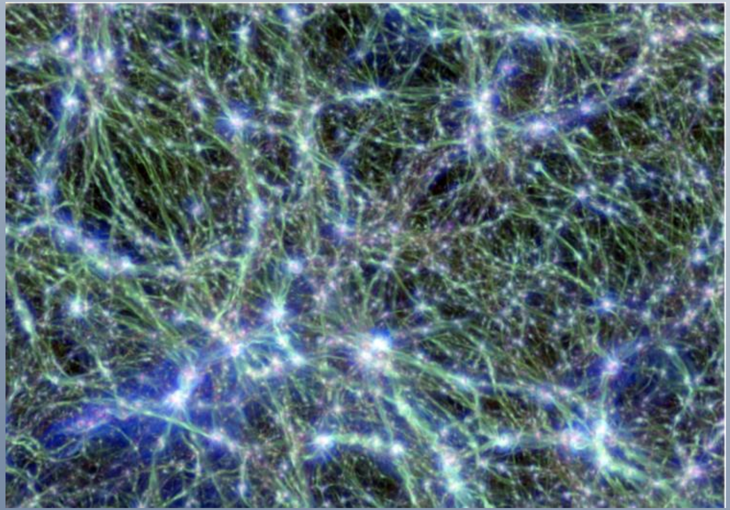

Vazza et al. 2018

Borlaff et al. 2021

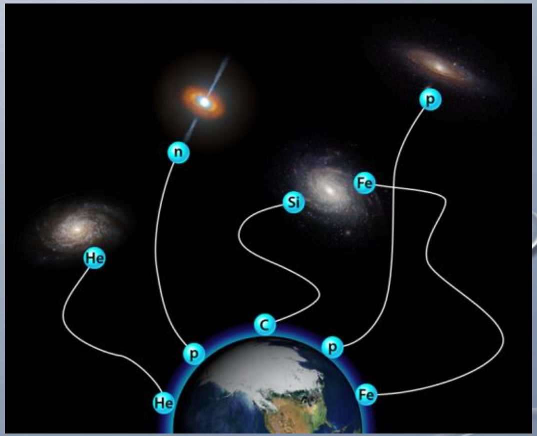

Credit: APSr

OBSERVATIONS: FERMI DATA

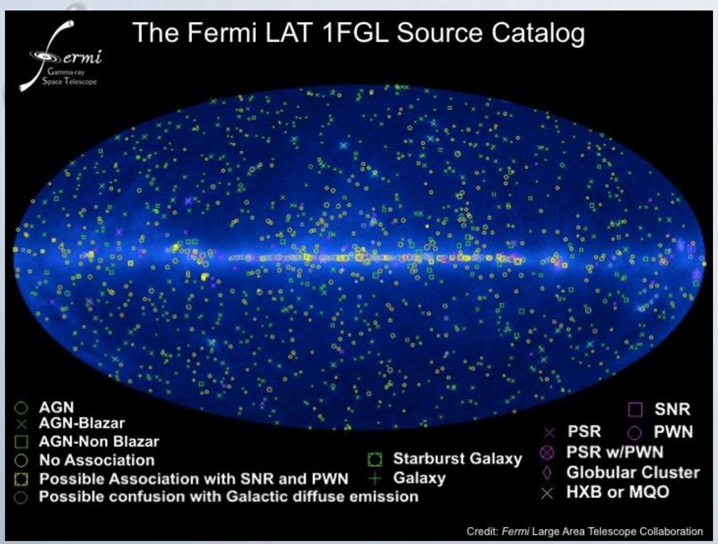

Credit FermiLAT

$$\gamma + \gamma \rightarrow e^{+} + e^{-}$$

A. Neronov & E. Vovk," *Evidence for Strong Extragalactic Magnetic Fields from Fermi Observations of TeV Blazars*", Science 328, 5974 (2010)

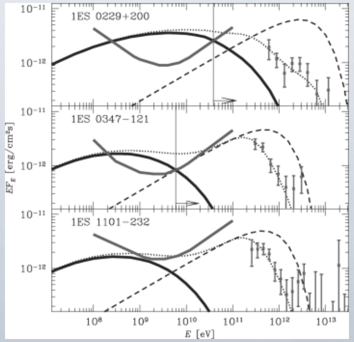

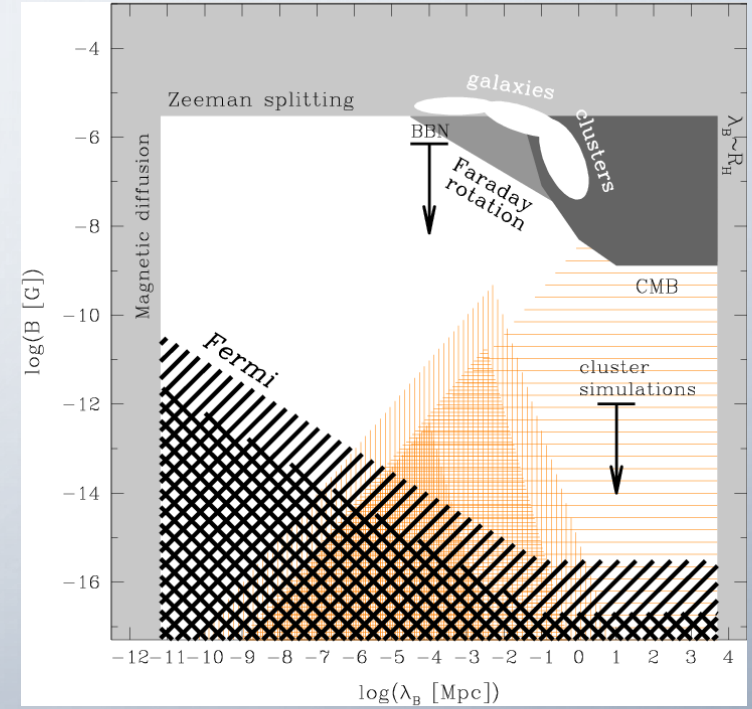

Bitteau, 2022

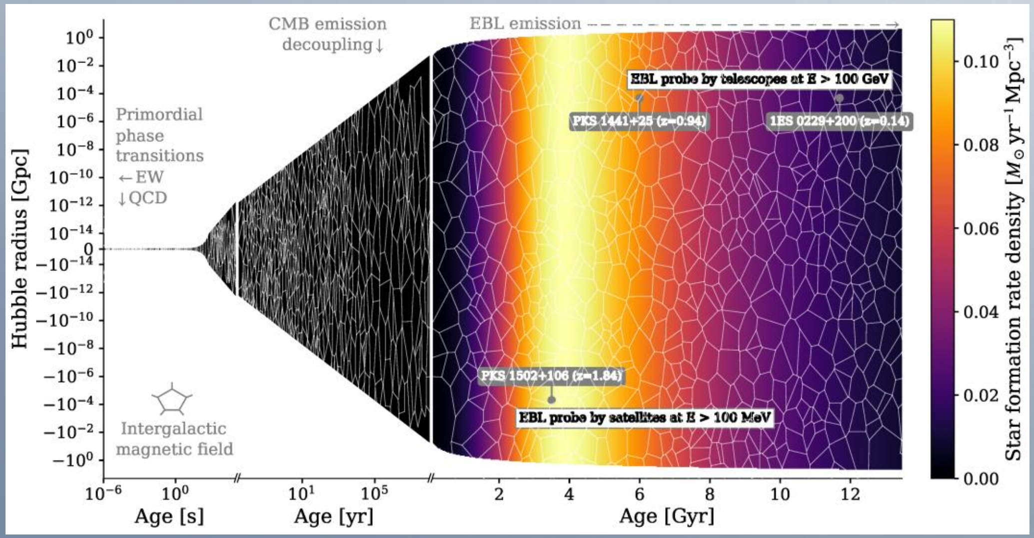

Dal Pino 2012

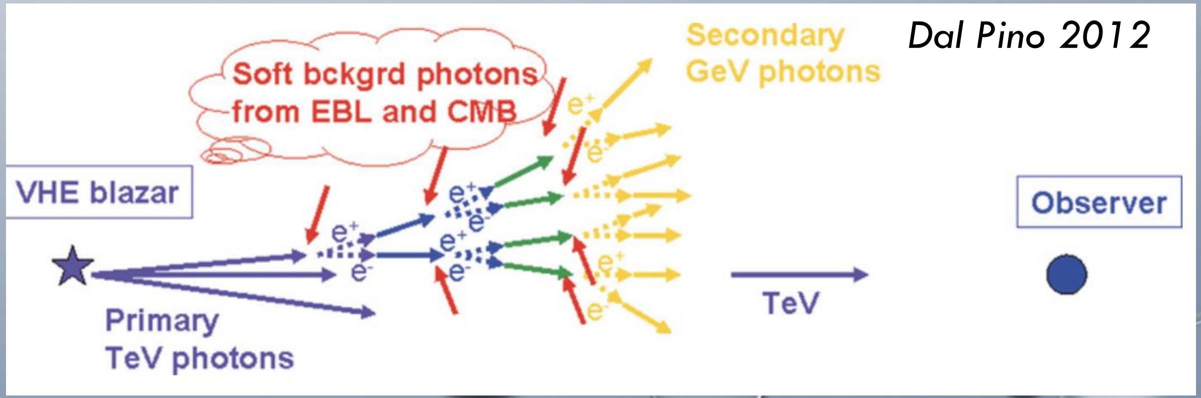

RECENT BLAZARS SPECTRA OBSERVATIONS:

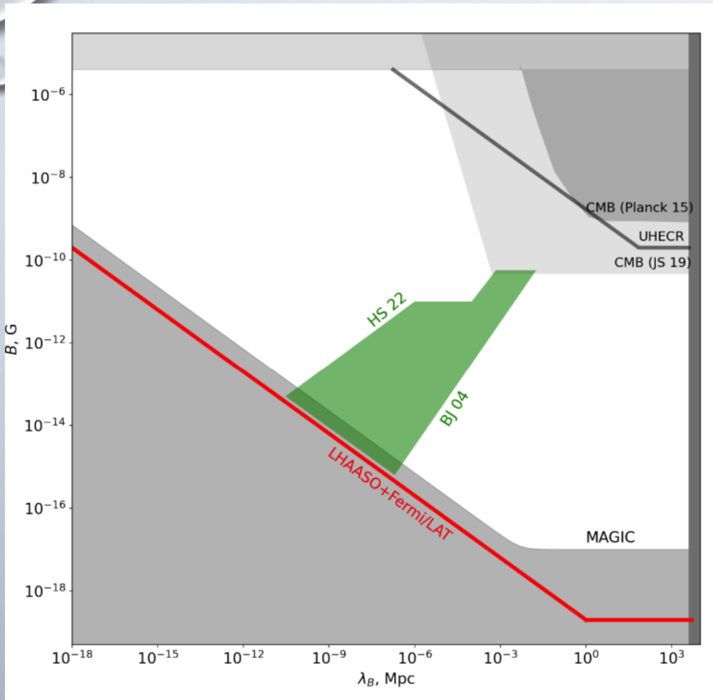

E. Vovk, et al. *"Constraint on intergalactic magnetic field from Fermi/LAT observations of the "pair echo" of GRB 221009A"* Astron.Astrophys. 683 A25 (2024)

Fig. 2. from Vovk et al. 2024: Lower bound on IGMF derived from the GRB 221009A (red line), compared to existing bounds form γ-ray, radio, CMB and UHECR observations and predictions of the cosmological evolution models. The CMB upper bounds are from Planck (Planck Collaboration et al. 2016) and from the analysis of Jedamzik & Saveliev (2019). UHECR upper bound is from Neronov et al. (2021). MAGIC lower bound is from Acciari et al. (2023). Green-shaded area shows the range of predictions for the endpoints of cosmological evolution of primordial magnetic fields. BJ04 is from Banerjee & Jedamzik (2004), HS22 is from Hosking & Schekochihin (2022).

Aharonian, F., et al. (Fermi-LAT, H. E. S. S), "Constraints on the intergalactic magnetic field using Fermi-LAT and H.E.S.S. blazar observations". Astrophys. J. Lett. 950, L16 (2023)

V. A. Acciari et al. [MAGIC Collaboration] "*A Lower Bound on Intergalactic Magnetic Fields from Time Variability of 1ES 0229+200 from MAGIC and Fermi/LAT Observations" Astron.Astrophys.* 670 A145 (2023)

S. Archambault et al. [VERITAS Collaboration], "*Search for Magnetically Broadened Cascade Emission From Blazars with VERITAS,*" Astrophys. J. 835, 288 (2017)

M. Ackermann, et al. [Fermi-LAT Collaboration], "*The Search for Spatial Extension in High-latitude Sources Detected by the Fermi Large Area Telescope,*" Astrophys. J. Suppl. 237 , 32 (2018)

GRAVITATIONAL WAVES FROM PRIMORDIAL TURBULENCE (AND/OR) MAGNETIC FIELDS

$$\nabla^2 \delta\rho(\boldsymbol{x},t) - \frac{1}{c_s^2}\frac{\partial^2}{\partial t^2}\delta\rho(\boldsymbol{x},t) = -\frac{\partial^2}{\partial x^i \partial x^j} T^{ij}(\boldsymbol{x},t), \qquad c_s^2 = \frac{\partial p}{\partial \rho}$$

$$\nabla^2 h_{ij}(\boldsymbol{x},t) - \frac{\partial^2}{\partial t^2} h_{ij}(\boldsymbol{x},t) = -16\pi G\, S_{ij}(\boldsymbol{x},t), \qquad c = 1$$

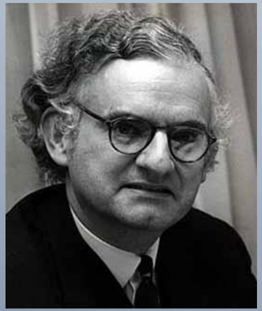

Aero-acoustic approximation:

- ✓ sound waves generation by turbulence
- ✓ gravitational waves generation

Lighthill, 1952; Proudman 1952

Kosowsky, et al, 2002, Dolgov, et al. 2002

Parameters:

τ_T turbulence lasting time

k_0 stirring scale

$M = v_0/c$ - Mach number

$R^{3/4} = k_d/k_0$ - Reynolds number

Gogoberidze, et al 2007

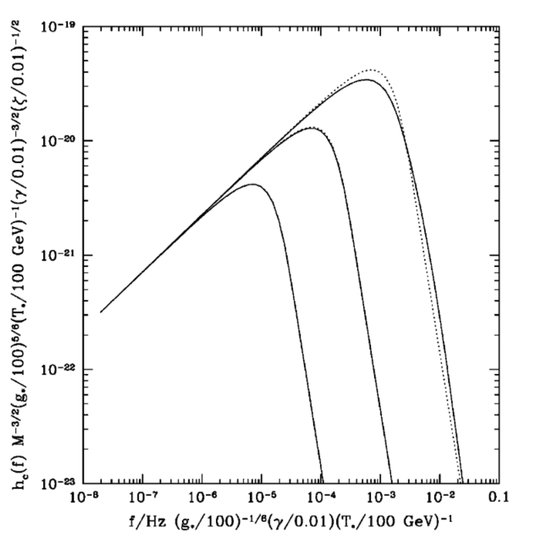

FIG. 1. The spectrum of gravitational radiation from turbulence. The three solid lines are for different Mach numbers, with $M = 0.01$, $M = 0.1$, and $M = 1$ from lowest to highest amplitude. Note that these three cases have also been scaled by a factor of $M^{-3/2}$ for display, since this is how the low-frequency tail scales with M. The dotted lines, which are virtually indistinguishable from the solid lines except for the $M = 1$ case, show the $k = 0$ approximation to the gravitational wave source.

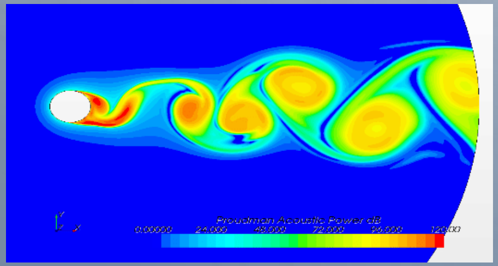

$$f = 1.65 \times 10^{-3}\,\mathrm{Hz}\left(\frac{\omega_*}{k_0}\right)\left(\frac{g_*}{100}\right)^{1/6}\left(\frac{\gamma}{0.01}\right)^{-1}\left(\frac{T_*}{100\,\mathrm{GeV}}\right),$$

$$\gamma H_*^{-1} = 2\pi/k_0, \qquad \zeta H_*^{-1} = \tau_T;$$

$$h_c(f) = 1.28 \times 10^{-19}\left(\frac{100\,\mathrm{GeV}}{T_*}\right)\left(\frac{100}{g_*}\right)^{1/3}\left(\frac{\gamma}{0.01}\right)^{3/2}\left(\frac{\zeta}{0.01}\right)^{1/2}\left[k_0^3\omega_*(f)H_{ijij}(\omega_*(f),\omega_*(f))\right]^{1/2}.$$

PROBING MAGNETOGENESIS SCENARIOS

- GRAVITATIONAL WAVES PROPAGATE ALMOST FREELY AND RETAIN THE INFORMATION ABOUT THE SOURCE AND PHYSICAL PROCESSES
  - FREQUENCY DETERMINES THE SOURCE CHARACTERISTIC LENGTH (TIME) SCALE
  - AMPLITUDES – THE SOURCE EFFICIENCY AND ENERGETICS.

$$f_{GW} = 2/l_S$$

$$N_b = \frac{H^{-1}}{l_S}$$

✓ If parity was violated -> helical turbulence
  - o Hydrodynamics (kinetic) turbulence
  - o MHD (magnetic dominant)

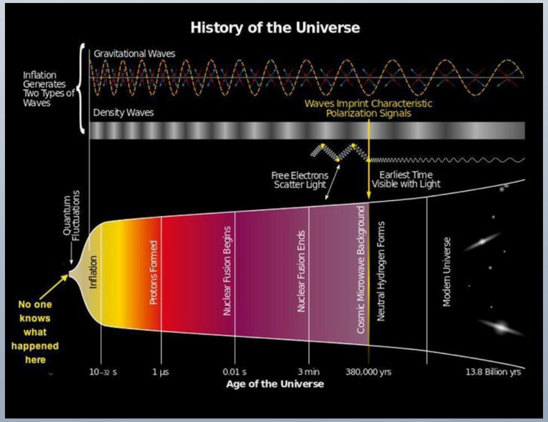

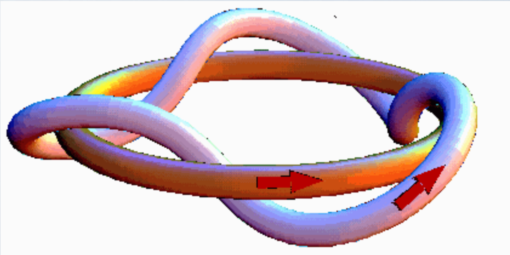

Magnetic helicity

$$H_B(t) = \int d^3x \mathbf{A} \cdot \nabla \times \mathbf{A},$$

✓ If the parity in the early universe is violated – relic gravitational waves are polarized.

WHY NUMERICAL MODELING NEEDED?

- ✓ TO ACCOUNT PROPERLY NON-LINEAR PROCESSES (MHD)
- ✓ NOT BE LIMITED BY THE SHORT DURATION OF THE PHASE TRANSITIONS
- ✓ TWO STAGES TURBULENCE DECAY
  - FORCED TURBULENCE
  - FREE DECAY
- ✓ THE SOURCE IS PRESENT TILL RECOMBINATION (AFTER THE FIELD IS FROZEN IN)
- ✓ RESULTS – STRONGLY INITIAL CONDITIONS DEPENDENT

$$\left(\frac{\partial^2}{\partial t^2} - c^2\nabla^2\right) h_{ij}^{\rm TT} = \frac{16\pi G}{a^3c^2} T_{ij}^{\rm TT},$$

Grishchuk 1974

$$\mathrm{d}t_{\rm phys} = a\mathrm{d}t \qquad h_{ij}^{\rm TT} = a h_{ij}^{\rm TT,phys}$$

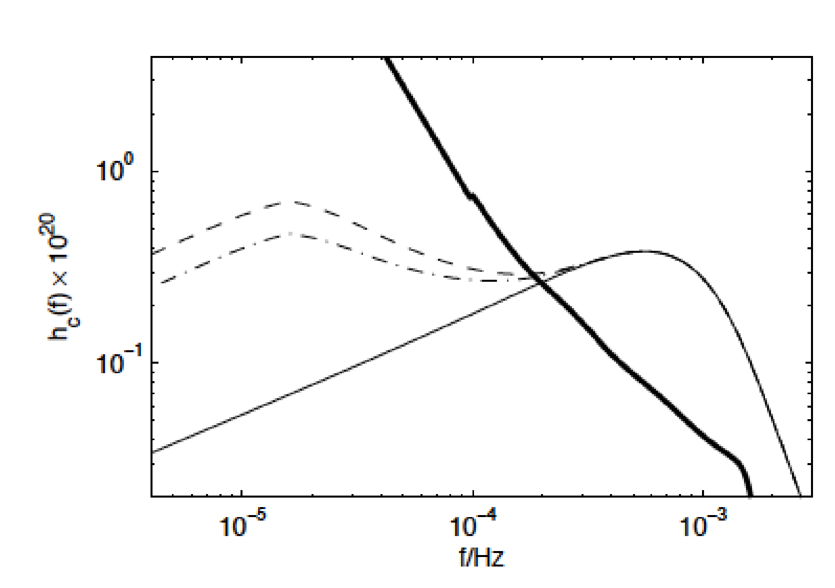

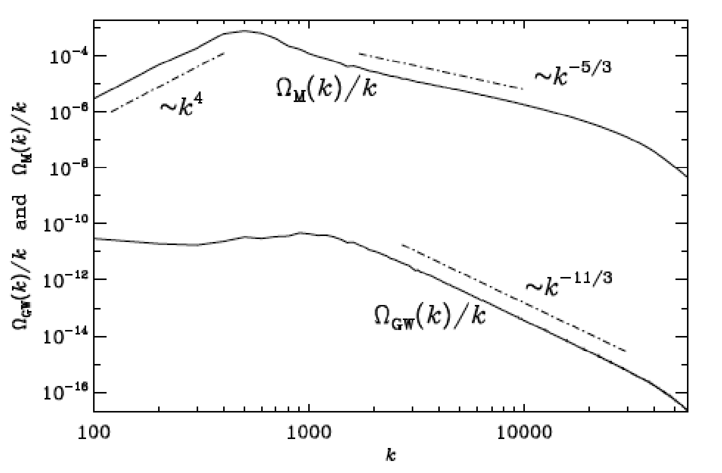

FIG. 2: Magnetic and GW energy spectra for run ini2 averaged over late times ($t > 1.1$), after the GW spectrum have started to fluctuate around a steady state, with $\Omega_M^{\max} \approx 0.12$ and $\Omega_{GW}^{\rm sat} \approx 2 \times 10^{-9}$.

Gogoberidze et al. 2007

Roper Pol et al. 2019,

WHY NUMERICAL MODELING NEEDED?

- ✓ IT IS ASSUMED THE STATIONARY TURBULENCE WHILE IN REALITY TURBULENCE DECAYS
- ✓ THREE STAGES OF GENERATION

$$\mathcal{E}_{\rm M}(t) = \mathcal{E}_{\rm M}^{\rm max}\,(1+\Delta t/\tau)^{-p}$$

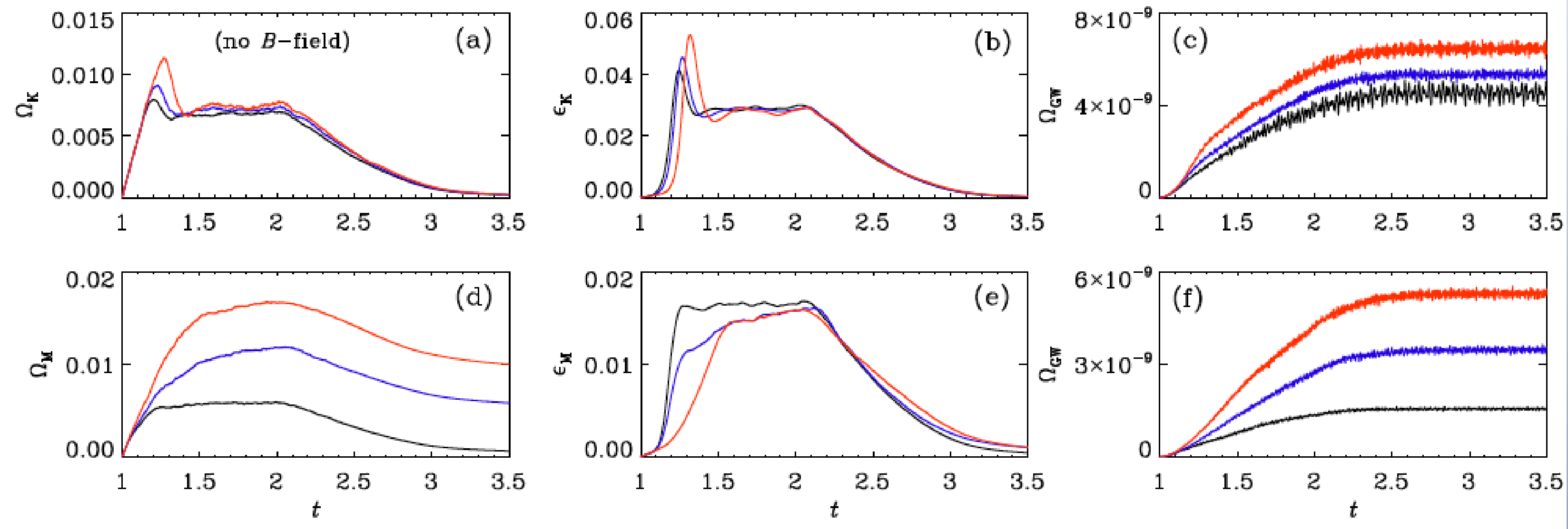

FIG. 2: Evolution of (a) $\Omega_{\rm K}$, (b) $\epsilon_{\rm K}$, and (c) $\Omega_{\rm GW}$ for kinetically driven cases with $\sigma = 0$ (black), 0.5 (blue), and 1 (red), and of (d) $\Omega_{\rm M}$, (e) $\epsilon_{\rm M}$, and (f) $\Omega_{\rm GW}$ for magnetically driven cases with $\sigma = 0$ (black), 0.3 (blue), and 1 (red).

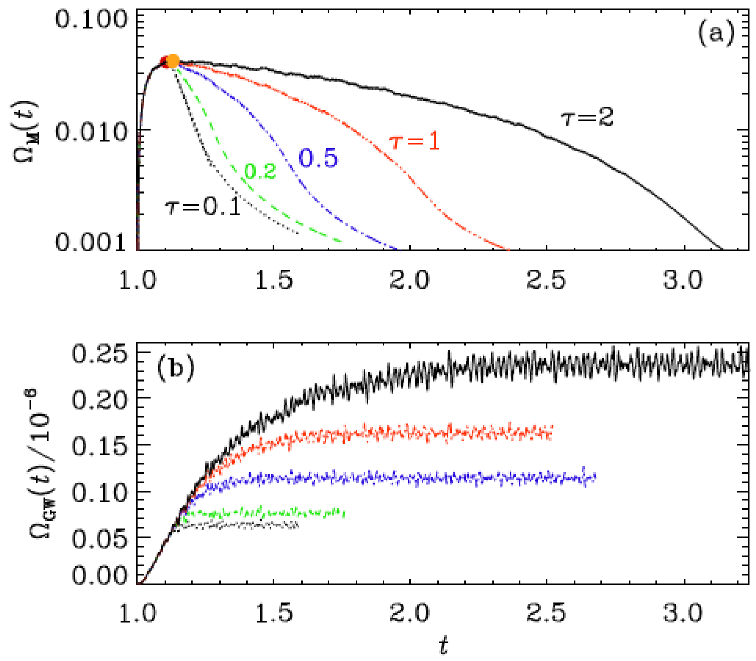

FIG. 1: Evolution of magnetic energy (top) and growth of GW energy density (bottom) for simulations where the driving is turned off at $t = 1.1$ (black dotted line), or the strength of the driving is reduced linearly in time over the duration $\tau = 0.2$ (green), 0.5 (blue), 1 (red), or 2 (black). Time is in units of the Hubble time at the moment of source activation.

Kahniashvili et al. 2020

PRIMORDIAL MAGNETIC FIELDS LIMITS FROM BBN

- EXTRA RADIATION LIKE ENERGY DENSITY LESS THAN ~3% OF THE RADIATION ENERGY DENSITY AT BBN

$$\frac{\rho_{\text{add}}}{\rho_{\text{rad}}} = 0.277\left(\frac{\Delta N_{\text{eff}}}{0.122}\right); \qquad \Delta N_{eff} = N_{\text{eff}} - N_{\text{eff}}^{\nu}$$

- THE UPPER BOUND ON THE MAGNETIC (EFFECTIVE) AMPLITUDE ORDER OF MICROGAUSS AT BBN
- ACCOUNTING FOR THE MAGNETIC FIELD DECAY:
  - THE MAGNETIC ENERGY DENSITY DOES NOT EXCEED THE RADIATION ENERGY DENSITY AT THE MOMENT OF GENERATION
  - BBN BOUNDS ARE SATISFIED

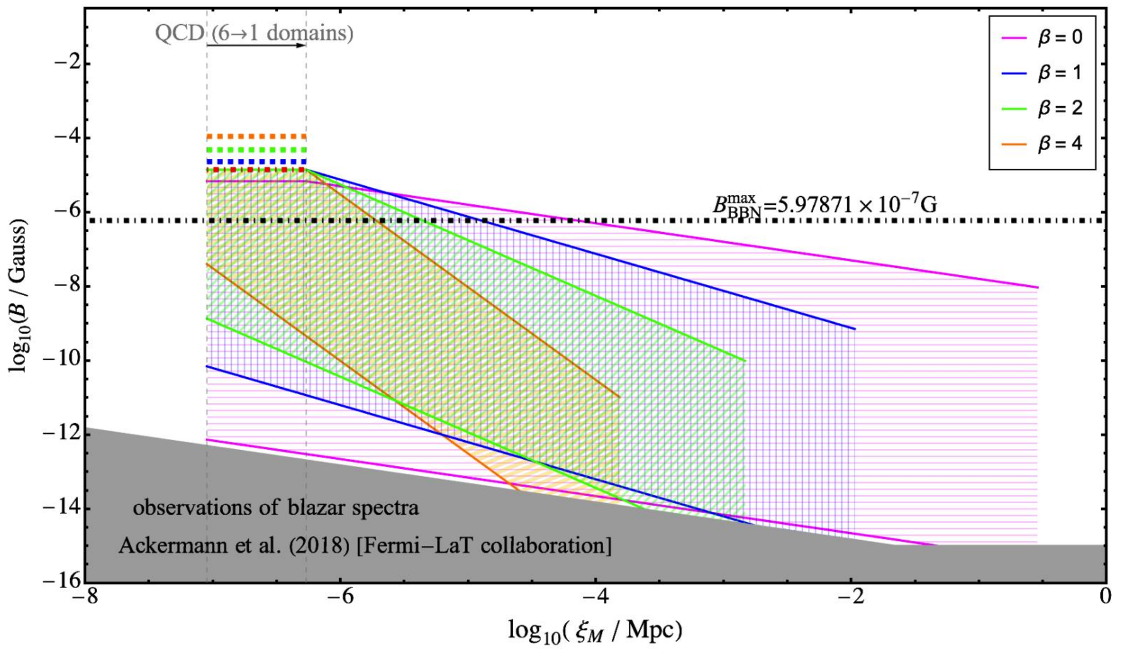

Figure 9: BBN bounds on the QCD phase transition generated initial field strength marked by horizontal dashed lines. For the non-helical cases, the initial energy density bound is more constraining than the BBN bound. Courtesy: Emma Clarke

Credit: Emma Clarke

GRAVITATIONAL WAVES FROM PRIMORDIAL TURBULENCE

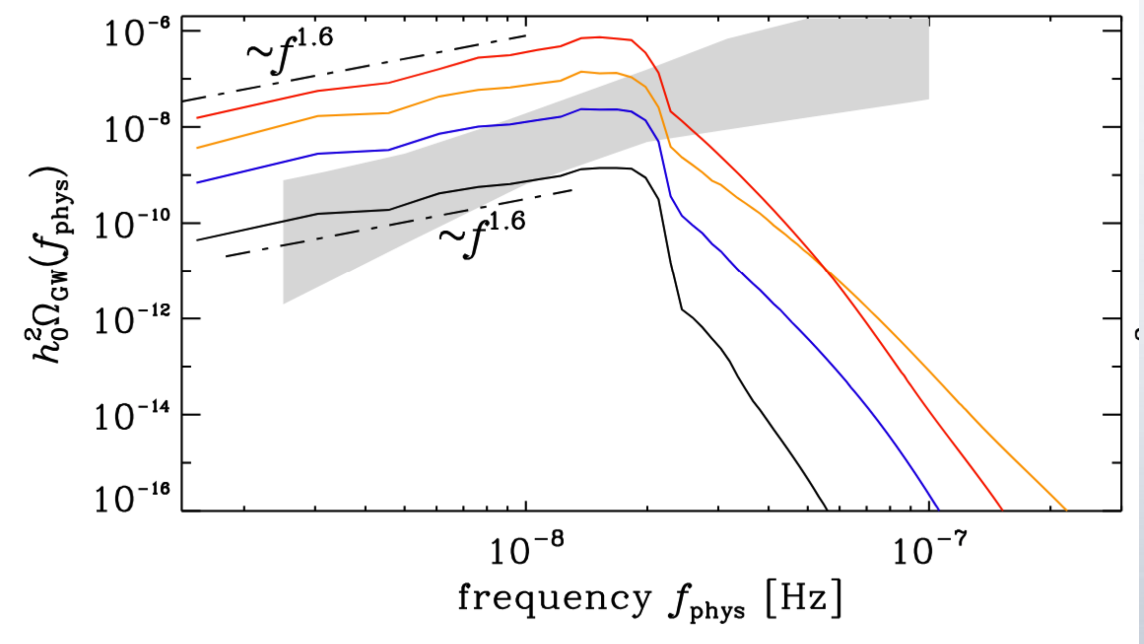

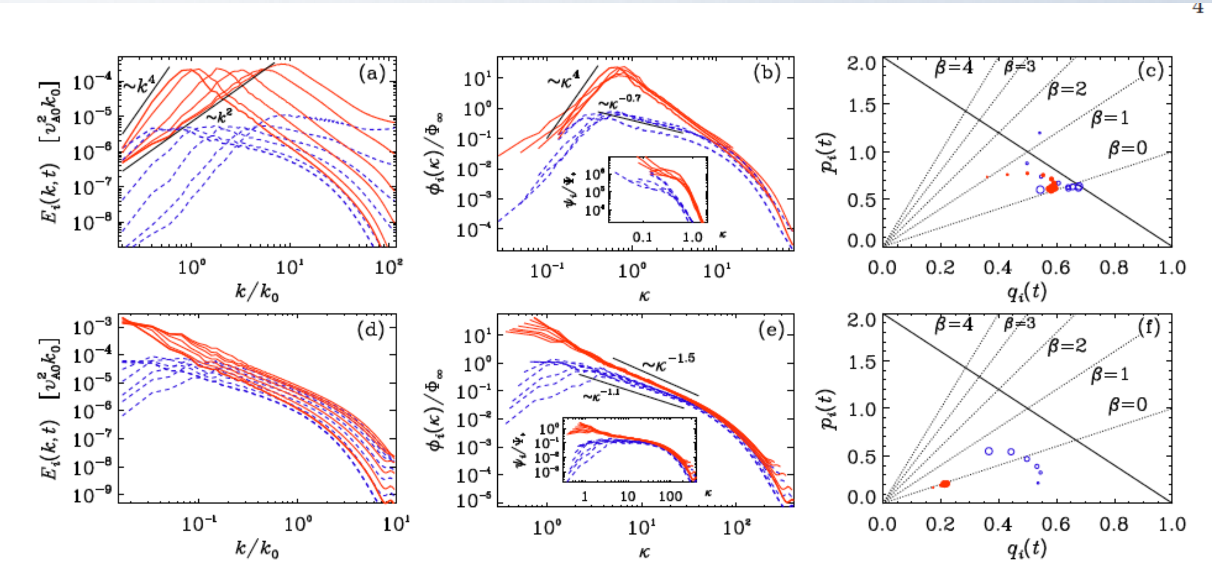

FIG. 3: $E_{\rm M}$ (solid) and $E_{\rm K}$ (dashed) in MHD with fractional helicity and $\alpha = 2$ (a), as well as full helicity and $\alpha = -1$ (d), together with compensated spectra (b,e) and the pq diagrams (c,f).

Brandenburg & Kahniashvili 2017

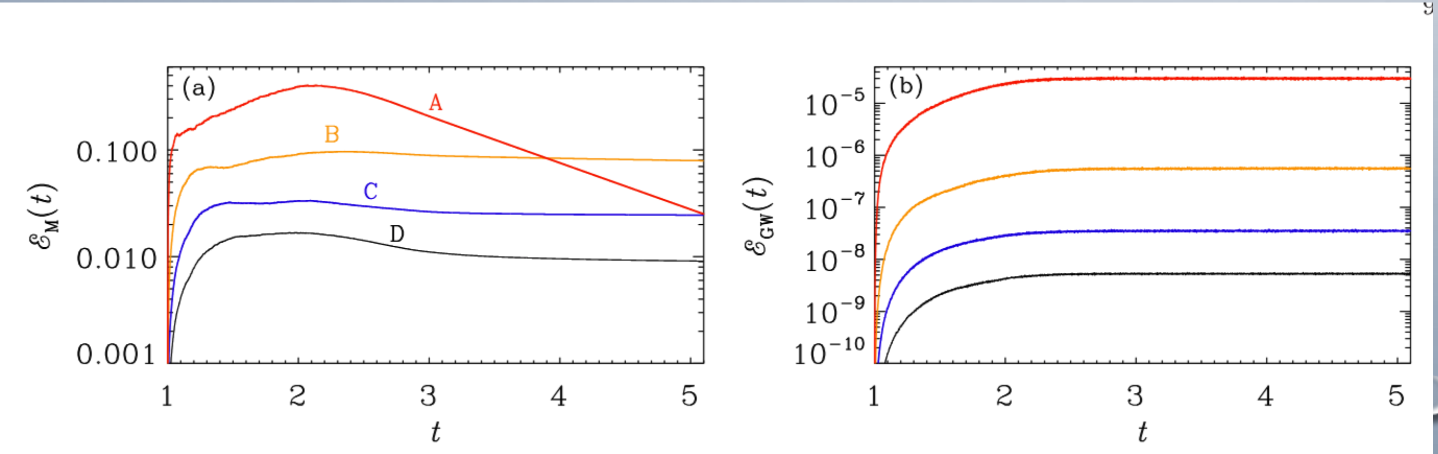

Kahniashvili et al. 2022

CONCLUSIONS AND TAKE HOME COMMENTS

- PTA OFFERS AN UNIQUE POSSIBILITY TO RECONSTRUCT THE INITIAL CONDITIONS AROUND QCD SCALE
- DETERMINE GRAVITATIONAL SIGNAL PROPERTIES THAT WILL ALLOW SEPARATION OF ASTROPHYSICAL AND COSMOLOGICAL BACKGROUNDS (ANISOTROPY, POLARIZATION, SPECTRAL SHAPE, NON-GAUSSIANITY…)
- IMPROVE THE MAGNETIC FIELDS OBSERVATIONS IN VOIDS AND FILAMENTS (TESTING MAGNOGENESIS MODELS)
- ADVANCE NUMERICAL SIMULATIONS TECHNIQUE TO MODEL PRIMORDIAL MAGNETIC FIELDS AND TURBULENCE; DETERMINE THE MECHANISMS INSURING THE PRESENCE OF VIABLE MAGNETIC FIELD/TURBULENT SOURCES IN THE EARLY UNIVERSE AND CORRESPONDINGLY CORRECT INITIAL CONDITIONS
- ADVANCE OUR UNDERSTANDING
    - ❖ PRIMORDIAL MAGNETOGENESIS
    - ❖ BUBBLE COLLISIONS/NUCLEATION – MORE REALISTIC MODELS
    - ❖ SOUND WAVES AS A SOURCE FOR TURBULENCE
    - ❖ AXIONS DRIVEN TURBULENCE AND AXION LIKE PARTICLES DRIVEN INFLATIONARY NEW PHYSICS

THANK YOU!

QUESTIONS? COMMENTS?

GRAVITATIONAL WAVES POLARIZATION

$$\mathcal{P}(k) = \frac{\langle h_+^\star(\mathbf{k})h_+(\mathbf{k}') - h_-^\star(\mathbf{k})h_-(\mathbf{k}')\rangle}{\langle h_+^\star(\mathbf{k})h_+(\mathbf{k}') + h_-^\star(\mathbf{k})h_-(\mathbf{k}')\rangle} = \frac{\mathcal{H}(k)}{H(k)}.$$

- ✓ POLARIZATION SPECTRUM RETAINS INFORMATION ON PARITY VIOLATION AT LARGE WAVELENGTHS
  - INVERSE CASCADING?

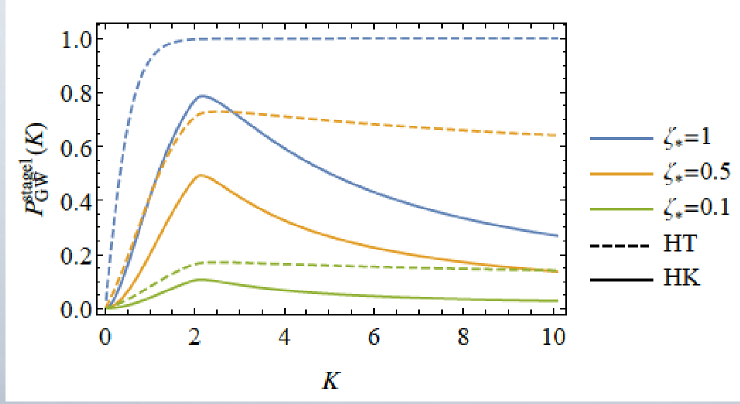

Ellis et al. 2020

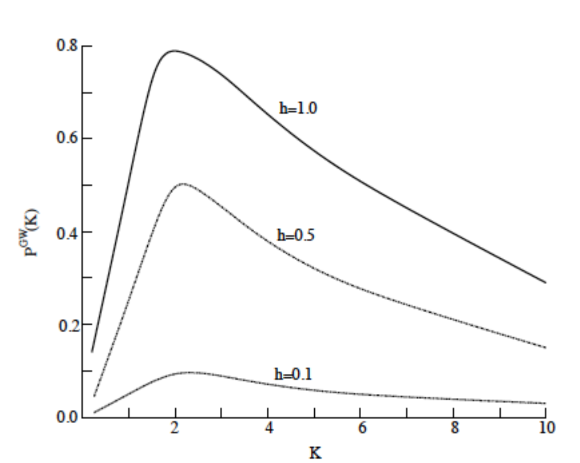

Kisslinger and Kahniashvili 2015

- ✓ ASSUMING *STATIONARY KOLMOGOROFF LIKE TURBULENCE* (HK) OR *STATIONARY HELICAL KOLMOGOROFF TURBULENCE* (HT)

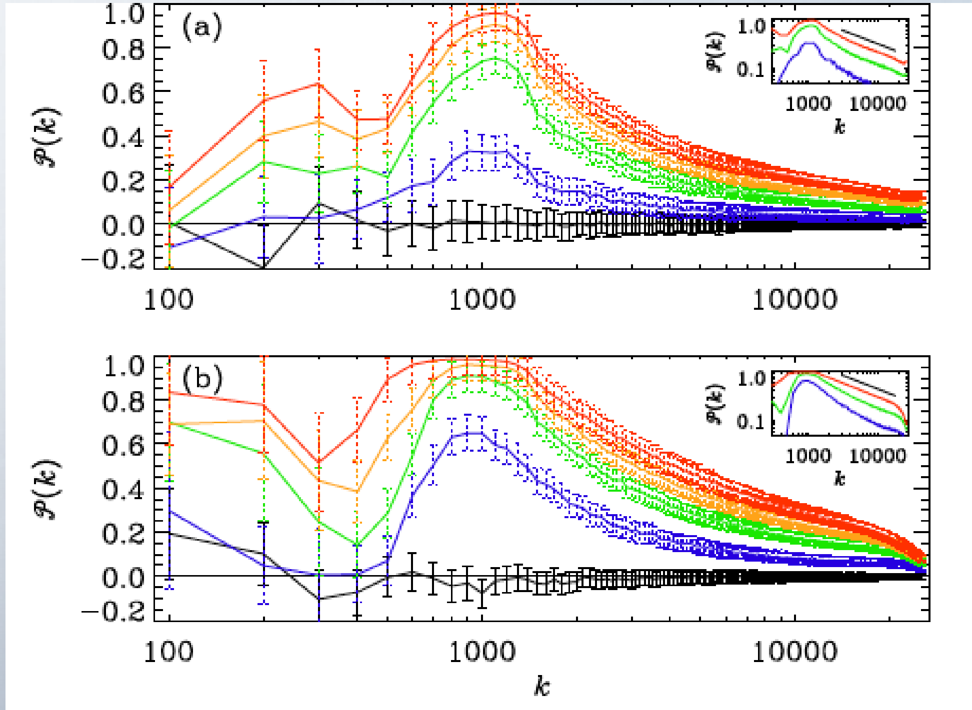

FIG. 3: Degree of circular polarization for (a) kinetically and (b) magnetically forced cases with $\sigma = 0$ (black) 0.1 (blue), 0.3 (green), 0.5 (orange), and 1 (red). Approximate error bars based on the temporal fluctuations and statistical spread for different random seeds of the forcing are shown as solid black lines for $\sigma = 0$ and as dotted lines otherwise.

Kahniashvili et al. 2020

GRAVITATIONAL WAVES FROM PRIMORDIAL TURBULENCE

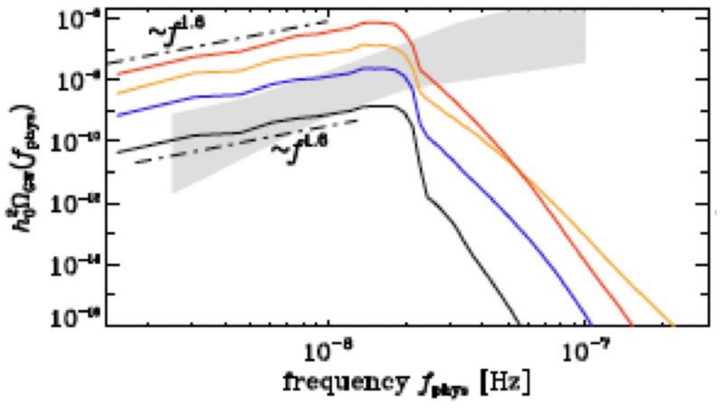

FIG. 2: Frequency spectra, $h_0^2\Omega_{GW}(f)$, for both the QCDPT
orange, blue, and black, respectively.

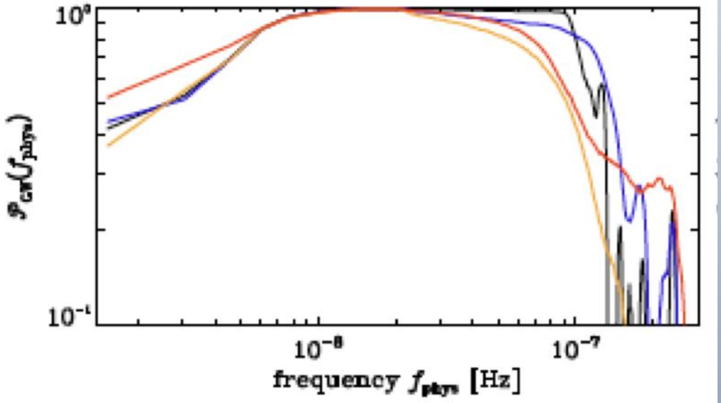

FIG. 3: Polarization spectra, $\mathcal{P}_{GW}(f)$, for the QCDPT Runs
orange, blue, and black, respectively.

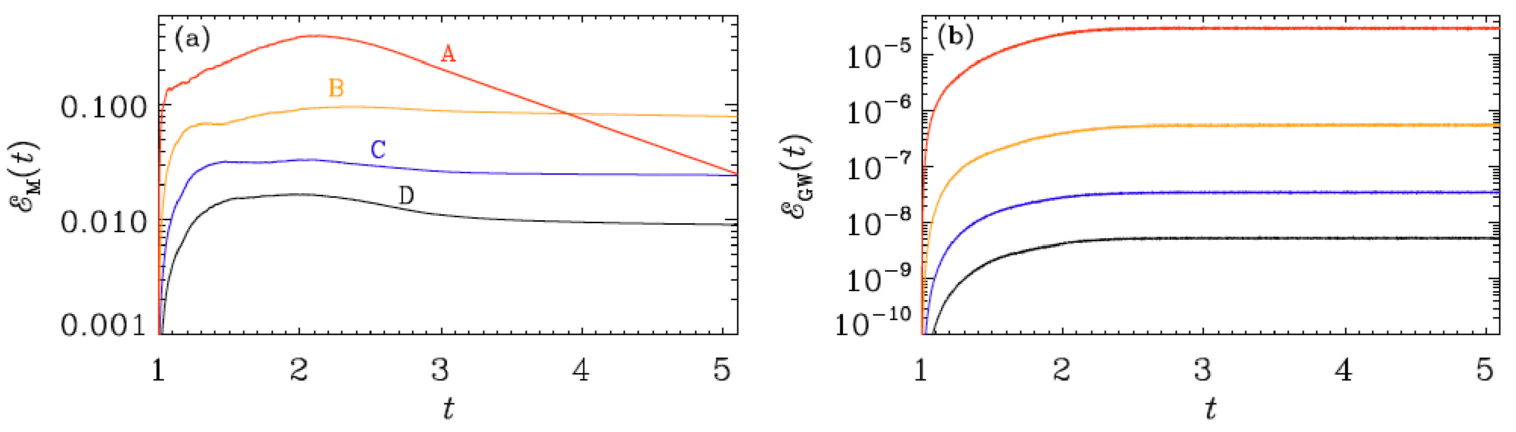

FIG. 6: Evolution of (a) $\mathcal{E}_M(t)$ and (b) $\mathcal{E}_{GW}(t)$ for Runs A–D of Table I. Note the rapid decay for Run A with the largest viscosity.

$$\mathcal{E}_{GW} = \left(q\frac{\mathcal{E}_M}{k_f}\right)^n$$

Kahniashvili et al. 2022